Left- and right-moving supercell dynamics, environments and hazards — today and in future

Monika Feldmann[1], Sandro Beer[1], Aaron W. Zeeb[2], Killian P. Brennan[3,a], Lena Wilhelm[1], and Olivia Martius[1]

[1]Oeschger Centre for Climate Change Research and Institute of Geography, University of Bern, Switzerland
[2]Department of Earth and Atmospheric Sciences, Central Michigan University, USA
[3]Institute for Atmospheric and Climate Sciences, ETH Zürich, Switzerland
[a]now at: Institute of Geography – Oeschger Centre for Climate Change Research

Correspondence: Monika Feldmann (monika.feldmann@unibe.ch)

Abstract. Supercell thunderstorms are among the most hazardous and damaging weather phenomena in Europe. However, little information is available on the relationship between supercell morphology and environmental conditions in Europe. We dissect supercell morphology, the changes in environmental conditions, and the subsequent changes in associated hazardous weather using numerical simulations of the current and a warmer climate at 2 km grid resolution. Comparing right- (RM) and

5 left-moving (LM) storms, we find that RMs have a more coherent storm structure and larger high-intensity areas, and their motion deviates stronger from the mean flow compared to LMs. LMs occur in a narrower range of environmental conditions, namely in hotter and less stable environments compared to RMs. Overall, in the warmer climate the pre-storm environment becomes less stable, and deep-layer shear increases. Accordingly, hazards associated with supercells such as lightning, wind gusts, intense precipitation, and hail size all increase. RMs and LMs reach similar hazard intensities, while RMs tend to

10 have larger high-hazard areas than LMs. The increase in hazard severity in the warmer climate is more pronounced for LMs, particularly for hail area and lightning intensity. A regional decomposition sheds further light on factors that influence the intensity of supercell hazards in different climate regions.

1 Introduction

Supercell thunderstorms are characterized by a persistent, rotating updraft and are widely recognized as the most hazardous

15 convective storm type (Markowski and Richardson, 2010). They frequently produce large hail, severe winds, torrential rainfall, intense lightning, and, rarely, tornadoes (Markowski and Richardson, 2010). Right-moving (RM) supercells, which deviate to the right of the mean wind vector and rotate cyclonically in the Northern Hemisphere, are more frequent and generally associated with a higher hazard intensity compared to their left-moving (LM) counterparts (that deviate to the left of the mean wind vector and rotate anticyclonically; Homeyer et al., 2025). Due to the higher occurrence rate, most supercell research

20 focuses on RMs (Zeeb et al., under review; Van Den Broeke et al., under review) and has led to little quantification and analysis of LMs in research that addresses future climate conditions (e.g., Feldmann et al., 2025a; Zeeb et al., 2024; Ashley et al., 2023). Though less frequent, LMs still represent an important fraction of the storm population and can be prolific hail

producers (Homeyer et al., 2025; Tonn et al., 2023). Considering that LMs have different life-cycles and often require a different environmental parameter space than RMs (Zeeb et al., under review; Homeyer et al., 2025), their response to a warming climate may also differ. Indeed, how both storm types respond to climate change is still subject to large uncertainties.

European research often focuses on severe convection in general rather than on supercells specifically. Previous studies on how severe convection changes with climate change faced several challenges. Reporting databases often suffer from sampling biases (Pîrloagă et al., 2021; Barras et al., 2019). Most radar networks undergo significant quality changes (Germann et al., 2022; Saltikoff et al., 2019), and their observational periods are typically too short for robust trend analyses (Wilhelm et al., 2024; Taszarek et al., 2021; Nisi et al., 2018). Proxy-based analyses in reanalysis or coarse-resolution climate models implicitly assume that the spatio-temporal distribution of storm environments reflects that of actual convection (Battaglioli et al., 2023), and they cannot capture structural changes in the storms themselves. Environmental analyses indicate that overall instability is expected to increase over large parts of Europe, while trends for deep-layer shear are more heterogeneous (Taszarek et al., 2021).

The emergence of kilometer-scale climate simulations allows studying explicitly resolved supercells in present and future climate simulations (Feldmann et al., 2025a; Ashley et al., 2023). Although these simulations remain limited to single realizations so far, they overcome many limitations of proxy studies and allow direct analyses of storm structure, environments, and hazards.

The preceding work of Feldmann et al. (2025a) uses two 11-year convection-permitting climate simulations over Europe: one representing the current climate and one using a pseudo-global-warming (PGW) approach corresponding to a +3 °C global warming level (GWL) relative to preindustrial levels (Cui et al., 2025; Thurnherr et al., 2025). Feldmann et al. (2025a) showed an overall increase in supercell frequency by 11% over Europe, with regional trends ranging from -28% to +116%, and frequency hotspots hugging the flanks of mountain ranges. Regional trends are tied to climatological moisture shifts, with frequency decreases being tied to an increasingly dry climate. Environmental analyses show an increase in both the frequency and magnitude of unstable conditions in the areas with the greatest positive trend, in agreement with Taszarek et al. (2021). The region with the largest decrease also shows decreases in unstable days and less potent convective conditions. Deep-layer shear during unstable conditions increases significantly over the majority of Europe, supporting the overall increase in supercell severity (Feldmann et al., 2025a).

Here, we use the same climate dataset for storm-centered analyses of storm morphology, surface hazards and pre-storm environments, over the whole European domain and in climatologically distinct sub-regions. Right- and left-moving supercells are tracked separately, allowing us to address the following research questions:

1. How do the frequency, structure, pre-storm environments, and hazards associated with RM and LM supercells differ in the present climate?

2. How do the environment and hazard characteristics change in a +3 °C warming scenario?

3. How do regional climate regimes affect this?

By explicitly analyzing RMs and LMs separately, this study reveals new insights into the fundamental characteristics of these two supercell types, as well as their future changes.

2 Materials and Methods

2.1 Data

60 We use km-scale climate model data from the COSMO-6 regional climate model, which was run at a 2.2 km resolution. In the current climate (CC) simulation (2011–2021), the boundary conditions are provided by ERA5 (Hersbach et al., 2020). The future climate (FC) simulation follows a PGW approach, using a GWL of +3°C (Brogli et al., 2023). A model member representative of convective summer precipitation of the MPI-HRES-ENS was chosen to compute the +3°C climate change Δ (Thurnherr et al., 2025). This climate change Δ is added to the ERA5 boundary conditions, mimicking the same 11-year

65 period and its variability in a warmed climate. Further details on the climate simulations and their verification are described in Cui et al. (2025); Thurnherr et al. (2025) and Feldmann et al. (2025a).

To identify supercells trajectories, supercell tracks from Feldmann et al. (2025a) are used. To identify supercells, first all thunderstorms are tracked based on 5-minute precipitation data (Brennan et al., 2024). Along these tracks, the hourly 3-D pressure-level wind field is used to apply vertical vorticity and updraft velocity thresholds in the mid-troposphere, identifying

70 the mesocyclone (for full documentation, see Feldmann et al., 2025a). The tracking differentiates cyclonic and anticyclonic updraft vorticity signatures, separating RM from LM supercells.

2.2 Methods

We use the cookie-cutter method introduced in Brennan et al. (2025). In this method, 3-dimensional environmental fields are extracted from the model data within a 60 km radius around each identified supercell at hourly intervals. Each extracted disk

75 is rotated so that the hourly smoothed propagation direction of the storm is due right (0°). The environmental data is extracted at the time of the storm, to reflect in-storm conditions, as well as 1 and 2 hours prior, to reflect pre-storm conditions. For each variable, we compute composites across all supercells or subsets of supercells for the current and future climate simulations separately.

Composite vertical profiles of the pre-storm environment are obtained from the extracted disks, with a filtering of active con-

80 vection via a precipitation filter of 5 mm h^{-1} with a 5-gridpoint circular buffer.

All statistical tests are performed with a two-sided Mann-Whitney-U test (p>0.05, McKnight and Najab, 2010), a non-parametric, unpaired test. Spatial analyses are additionally processed with a false-discovery-rate (FDR) correction (Ventura et al., 2004; Benjamini and Hochberg, 1995).

Analyses of storm motion make use of the Bunkers storm motion estimate (Bunkers et al., 2000) for RMs (eq. 1) and LMs (eq.

85 2):

$$\mathbf{V}_{\mathrm{RM}} = \mathbf{V}_{\mathrm{mean}} + \mathrm{C}_{\mathrm{RM}} \frac{\hat{\mathbf{k}} \times \mathbf{S}}{\|\mathbf{S}\|} \tag{1}$$

$$\mathbf{V}_{\mathrm{LM}} = \mathbf{V}_{\mathrm{mean}} - \mathrm{C}_{\mathrm{LM}} \frac{\hat{\mathbf{k}} \times \mathbf{S}}{\|\mathbf{S}\|} \, , \tag{2}$$

where $\mathbf{V}_{\mathrm{mean}} = \frac{1}{\Delta p} \int_{925\,hPa}^{500\,hPa} \mathbf{V}(p)\,\mathrm{d}p$, $\mathbf{S} = \mathbf{V}_{500\,\mathrm{hPa}} - \mathbf{V}_{925\,\mathrm{hPa}}$, $\hat{\mathbf{k}} = (0,0,1)$, and $\mathbf{S}_{\perp} = \frac{\hat{\mathbf{k}} \times \mathbf{S}}{\|\mathbf{S}\|}$, here adapted to pressure-level model data. Originally both C_{RM} and C_{LM} were estimated at 7.5 m s^{-1} (Bunkers et al., 2000), while Bunkers et al. (2024) suggests an updated C_{LM} of 5 m s^{-1}.

3 Results

The tracking identifies ∼8200 right-moving hourly supercell detections and ∼1200 left-moving ones in the current climate simulations. While observational studies do suggest a majority of RM storms (75%, Tonn et al., 2023), we consider the modeled fraction of 87% to likely be an overestimation of the true RM fraction, because of the shorter lifetime of LMs, which are hence more likely to be missed by the hourly detection interval (Zeeb et al., under review; Wade and Parker, 2021; Sherburn et al., 2016; Sherburn and Parker, 2014).

In the warmer climate, RMs increase by 8% to ∼8900 detections and LMs by 21% to ∼1500 detections, resulting in a slight increase in the LM fraction from 13% to 14% [1].

3.1 Supercell structure

Figure 1 compares the storm morphology of right- and left-moving supercells based on composites of precipitation, vertical velocity, and vorticity. Overall, the composites show strongly smoothed storm structures, owed to the averaging across many cases. RM storms exhibit the familiar right-leaning curvature of the 15 mm h^{-1} precipitation contour, with the mesocyclone located at the inner corner of this curve (center of the cookie). LM storms show a weaker and less elongated leftward curvature of the precipitation field. To identify the updraft, we show the 90th percentile of 500 hPa vertical wind and 500 hPa vertical vorticity (10th percentile of vertical vorticity for the LMs, due to the opposite sign of the vorticity). Midlevel updraft and vorticity extrema are both in the center of the composite. The updraft and vorticity signatures are of similar size and intensity in both storm types. The downdraft features are depicted by extracting the 10th percentile of the 700 hPa vertical wind and 500 hPa vertical vorticity (90th for the LMs). Similar to the updraft, the downdraft intensity and area are comparable in the RM and the LM. Precipitation largely falls in the respective downdraft regions. The vorticity in the downdraft area is more pronounced on the LMs than the RMs. Despite the less pronounced shape in the mean precipitation contour, LMs still show a clearly identified updraft area in the center of the composite, and a downdraft area at the right-hand storm flank, that mirror the

---

[1]Discrepancies with the changes shown in Feldmann et al. (2025a) are owed to computing the RM/LM fraction and their changes based on complete tracks, in comparison to all hourly detections, as done here. Changes in track duration and rotation persistence throughout the track cause these differences.
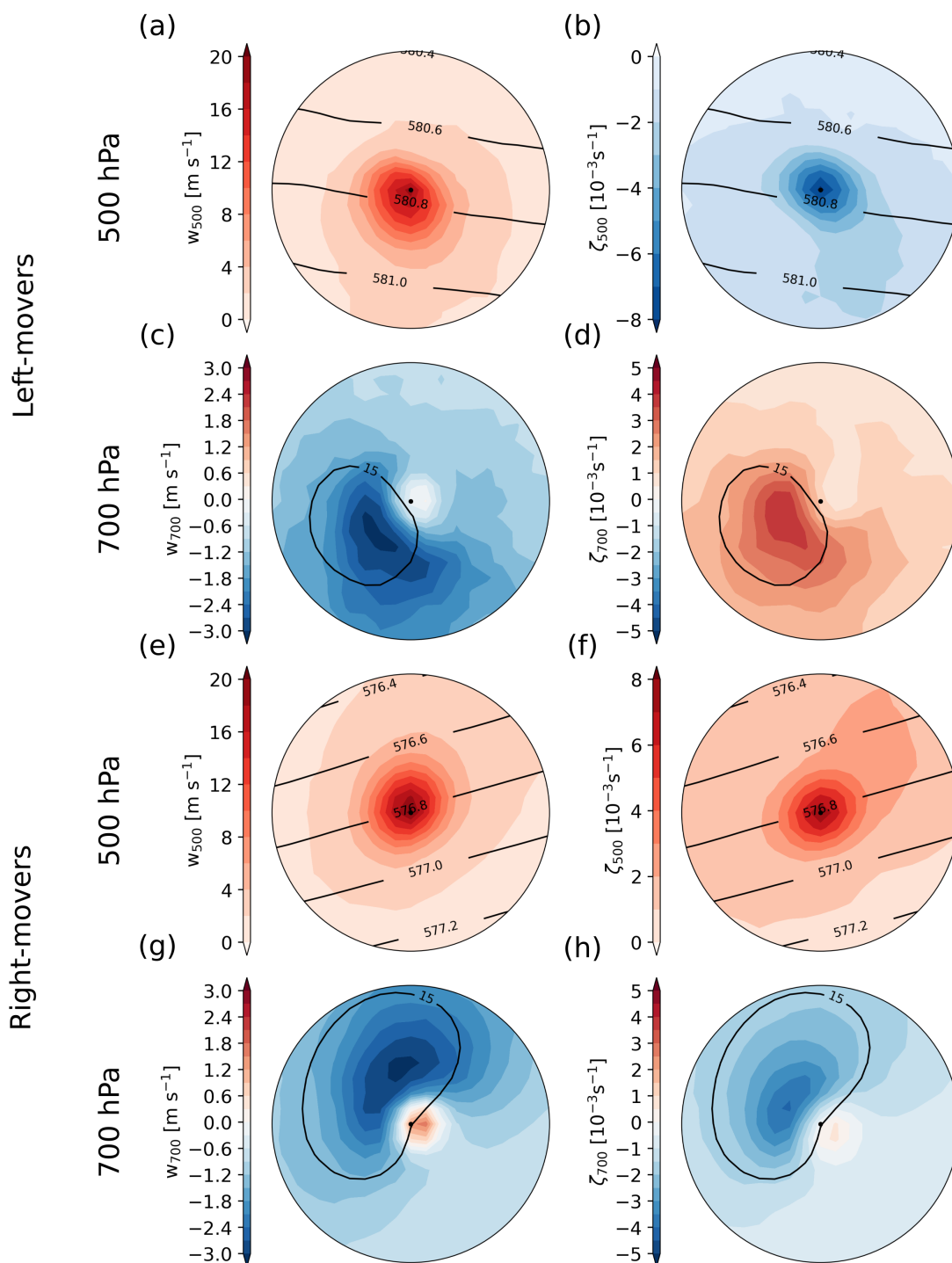
Figure 1. Structure of LMs (top rows) and RMs (bottom rows) in the current climate. The "cookies" (radius 20 km) show grid-point wise percentile values across all LM or RM cases and across all time steps. For the updraft metrics we show the 90th percentile at the 500 hPa level, for the downdraft metrics we show the 10th percentile at the 700 hPa level. Composite mean geopotential height at 500 hPa (dam) and mean precipitation rate ($mm\,h^{-1}$) are shown in black contours.
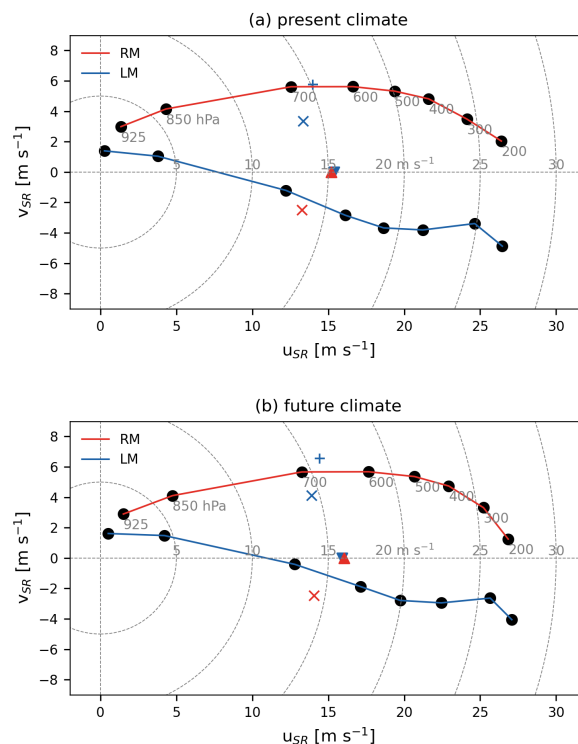
Figure 2. Composite storm-direction-relative (SR) hodographs in the current (a) and future (b) climates. In the hodographs, observed storm motion is indicated with a colored triangle, Bunkers motion with an x (current recommendation c = 7.5 m s^{-1} for RM and 5 m s^{-1} for LM) or a + (old recommendation c = 7.5 m s^{-1} for LM)

structure of the RMs and rival them in terms of intensity (e.g., Davies-Jones, 2015).

To investigate the synoptic meteorological situation, we look at the composite of geopotential height at 500 hPa 2h before storm-encounter, to ensure unperturbed conditions—one hour prior and hour zero were tested and showed considerable in-
115 fluence of the presence of the storm. Both storm types deviate to the right and left of the isohypses, respectively, consistent with their deviant motion. The isohypses also indicate a low-pressure area lying to the left-hand side of storm motion and higher pressure being on the right-hand side. The gradient of geopotential height is greater in the RMs, while also being at a lower geopotential height. Severe convection in Europe typically occurs at the leading edge of an approaching trough and in southwesterly flow (Feldmann et al., 2025b; Wapler and James, 2014), consistent with the pattern of geopotential height. The
120 greater height and weaker gradient for LMs indicate that they may be preferentially located closer to the downstream ridge. This behavior will be discussed further in Section 3.2.

3.2 Supercell environments

A priori, we expect the biggest differences between RM and LM supercell environments in their respective pre-storm hodographs (e.g., Bunkers, 2002; Bunkers et al., 2000; Houze et al., 1993). The environmental conditions are extracted 1h pre-storm en-

125 counter (see Fig. 2), which yielded the most representative (i.e., least convectively contaminated and highest convective potential) results. The hodographs are rotated so that storm motion is aligned among all of them, yielding storm-direction-relative (SR) u_{SR}- and v_{SR}-components of the profile, u_{SR} being along the propagation direction and v_{SR} perpendicular to it, i.e. modeled storm motion lies on the v_{SR}=0 line.

The hodographs of RMs in the current climate (Fig. 2a) exhibit a slight clockwise curvature with altitude, while overall being

130 largely straight, with storm motion lying to the right of the hodograph. Shear is largely concentrated at the 850-700 hPa level, whereas the near-surface change in wind speed is very gradual. The LMs' hodograph has a lower degree of counterclockwise curvature with slight veering in the low-levels and virtually identical deep-layer shear (e.g., Zeeb et al., under review; Bunkers et al., 2024; Tonn et al., 2023; Bunkers, 2002; Bunkers et al., 2000). Both mean hodographs are mostly straight and do not exhibit large degrees of directional shear (Fig. 2). At a 3°C warming level (Fig. 2b), both hodographs lengthen and the 925-500

135 hPa shear increases by 1-2 m s^{-1}.

Modeled storm motion was extracted from the 5-min precipitation tracks and smoothed with a moving-average 5-timestep window. We compare modeled storm motion ($v_{SR} = 0$ m s^{-1}) to the estimated Bunkers storm motion (Bunkers et al., 2024, 2000, see equations 1 and 2) using both the $C_{RM,LM} = 7.5$ m s^{-1} and $C_{LM} = 5$ m s^{-1} constant. While the obtained velocity is comparable, albeit slightly smaller than the modeled storms, the estimated deviation from the mean flow is considerably larger

140 than in the modeled storms. By refitting C to scale estimated storm motion onto the $v_{SR} = 0$ m s^{-1} line, our simulations suggest an RM offset of $C_{RM} = 5$ m s^{-1} and an LM offset of $C_{LM} = 1$ m s^{-1}.

In addition to the composite hodographs, we investigate the mean propagation direction and speed in Fig. 3. In line with previous studies showing that severe convection in Europe happens overwhelmingly during SW flow (Feldmann et al., 2021; Mohr et al., 2020; Wapler and James, 2014), supercells track largely towards the NE (see Fig. 3a). There is a distinct separation

145 of the mean track direction of right- and left-movers by 12°, with the mean track of RMs lying to the right of the LMs, as expected. The angle difference between the storm types suggests that they form in different systematic locations of synoptic systems (e.g., the hodograph shape and subsequent mean wind vector are different at the base of the trough versus the top of the ridge). Both storm populations track 3° more northwards in the future climate (Fig. 3a). From Fig. 3b we further see that propagation speed is comparable between RMs and LMs, with an average of approximately 15 m s^{-1}. In line with the increase

150 in deep-layer shear and the lengthening of the hodograph, the propagation speed increases by ∼1.5 m s^{-1} at the 3°C GWL.

We investigate the thermodynamic environment both in a composite skew-T log-p diagram (see Fig. 4) and by comparing the distribution of composite environmental parameters (see Figs. 5). The skew-T diagram (Fig. 4) shows significant differences between RM and LM in the current climate. LMs occur in significantly warmer conditions, with higher lifting condensation levels (LCL) and higher CAPE and CIN values than RMs. Low-level specific humidity is also slightly higher for LMs, but

155 relative humidity is lower due to the large temperature difference of almost 3°C. This poses the question, why LMs occur
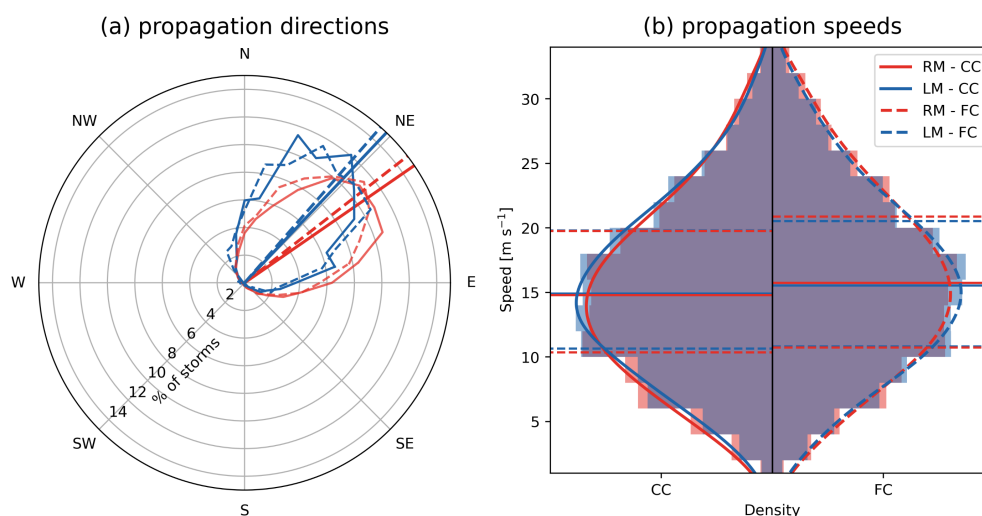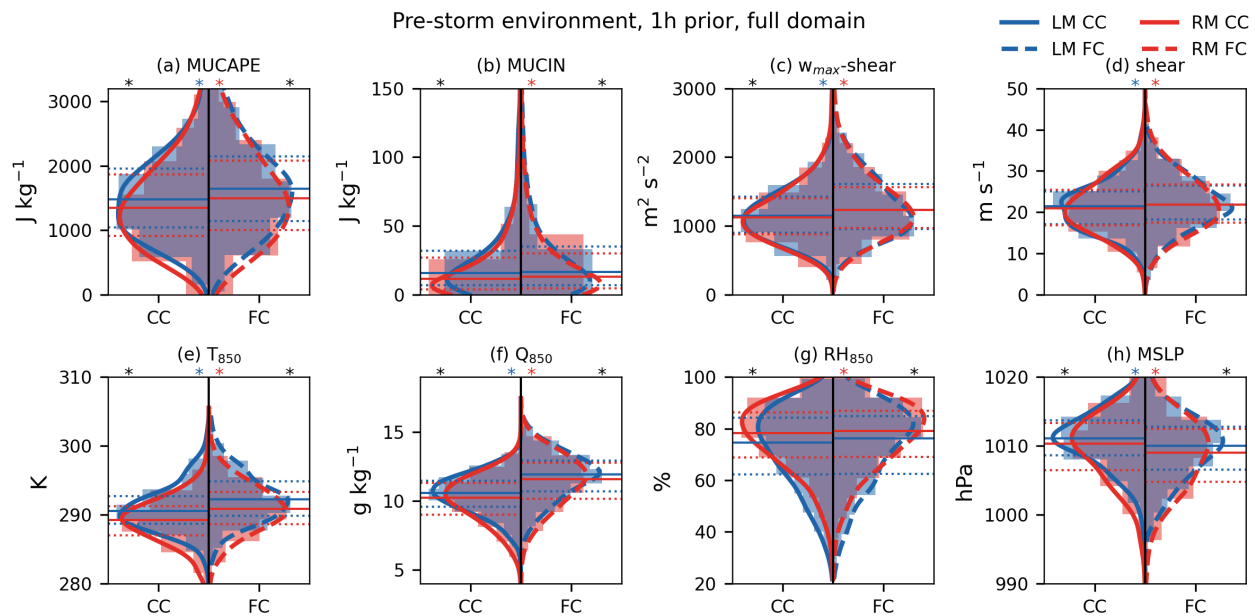
Figure 3. Density distributions of propagation a) direction and b) speed, solid lines indicate current climate (CC) and dashed lines future climate (FC), blue corresponds to LM and red to RM. In panel b), the interquartile range is indicated in dotted lines, the median with a solid line, CC is depicted on the left-hand side, and FC on the right-hand side.
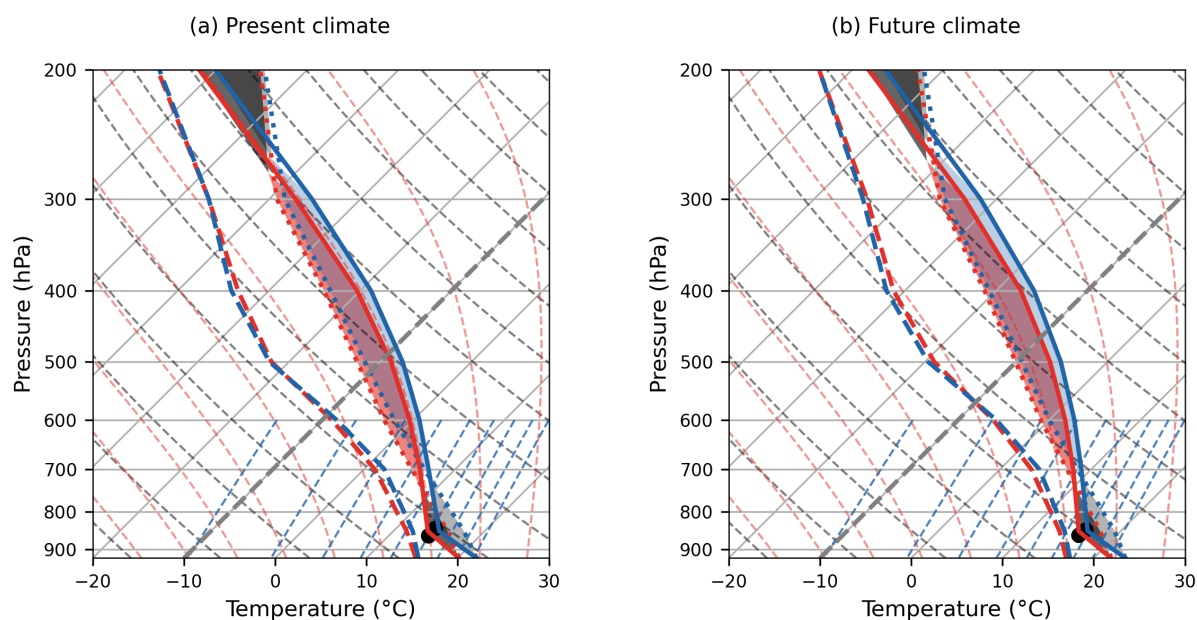

Figure 4. Composite skew-T log P diagrams of LMs (blue lines) and RMs (red lines) in the current (left) and future (right) climates.

Figure 5. Density distributions of 1h pre-storm environment, interquartile range is indicated in dotted lines, the median with a solid line. The current climate (CC) is depicted on the left-hand side of each plot, the future climate (FC) on the right-hand side. Significant differences between the LMs are indicated with a blue asterisk, between the RMs with a red asterisk, between the current climate with a black asterisk on the left, and between the future climate with a black asterisk on the right.

in such thermodynamically different conditions. Comparing the distribution of CAPE, CIN, deep-layer shear, and low-level atmospheric conditions for RM and LM (Fig. 5), we see that LM-supporting conditions have lower variability than those of RMs, with a narrower interquartile range. Given that LMs occur more rarely, it appears that LMs require a more specific range of environmental conditions (Fig. 5). In the seasonal and diurnal cycle, LMs occur more frequently during the convective peak

160   season, and less frequently in the shoulder seasons, showing a sharper peak in the distribution, with shorter tails (see Fig. 6a). During the convective peak season, instability and temperature are generally greater than in the less favorable shoulder seasons and nighttime hours. Additionally, LMs occur in significantly higher mean surface pressure situations than RMs (see Fig. 5h), and their surroundings show smaller surface pressure gradients (not shown). This indicates that, from a synoptic perspective, they occur closer to the center of the ridge, further supporting the hypothesis from Section 3.1. Overall, severe convection in

165   Europe predominantly occurs between an upstream trough and a downstream ridge (Feldmann et al., 2025b). In this transition area, warm air advection may occur in the warm sector ahead of the cold front. Warm air advection induces a vertical clockwise turning of the geostrophic flow, due to thermal wind balance. Closer to the center of the ridge, wind speeds are lower and hence warm air advection is smaller, hence producing less synoptic forcing towards a clockwise turning hodograph, which favors RMs (Houze et al., 1993; Peyraud, 2013; Davies-Jones, 1984, 2002).
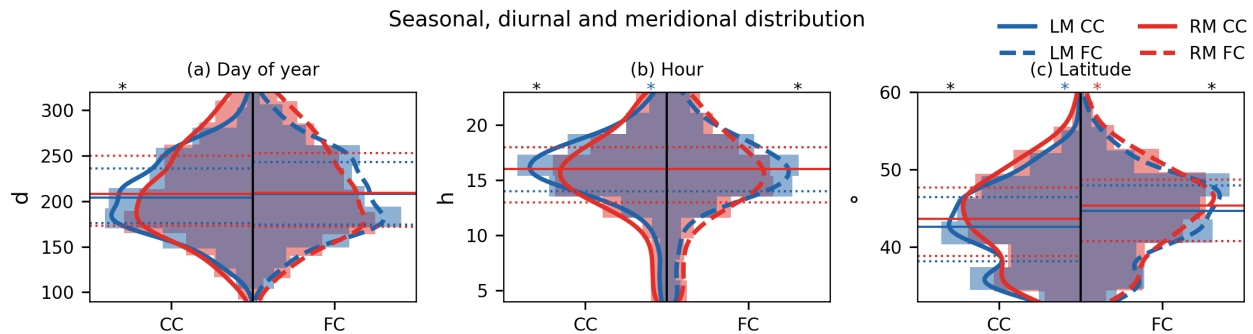
Figure 6. Empirical PDF of seasonal and diurnal cycle, as well as longitudinal distribution of LMs (blue) and RMs (red) in the current (solid lines, left) and future climate (dashed lines, right). Significant differences between LMs and RMs are marked with an asterisk, the median is depicted with a solid line and the interquartile range dotted.

In a 3°C warmer atmosphere, the thermodynamic profiles for both RMs and LMs show an increase in temperature and specific humidity (see Figs 4 and 5). Focusing on the vertical profiles of the RMs, separate factors contributing to both increases can be decomposed. With a surface temperature increase and a low-level specific moisture increase, the LCL remains approximately stable (see Table 1). Due to the steeper moist adiabatic lapse rate at warmer temperatures, the level of free convection (LFC) increases slightly. The environmental lapse rate is stabilizing slightly; however, the steeper moist adiabat over the full vertical range from the surface to the LFC for CIN and from the LFC to the level of neutral buoyancy (LNB) for CAPE compensates this and increases the area of the integral. While relevant environmental intensity metrics increase for both right- and left-movers (Fig. 5), the increase tends to be even greater for LMs, with larger changes in CAPE, surface temperature, and specific humidity.

**Table 1.** Thermodynamic mean state and mean climate change Δ from pressure levels

	CAPE [J kg^{-1}]	CIN [J kg^{-1}]	LFC [hPa]	LCL [hPa]	Q$_{925}$ [g kg^{-1}]	RH$_{925}$ [%]	T$_{925}$ [°C]
LM - CC	982	-71	721	833	12.0	67	22.7
RM - CC	842	-42	744	855	11.8	73	20.6
LM Δ FC-CC	+117	-7	-4	+2	+1.4	+1	+1.9
RM Δ FC-CC	+95	-6	-9	-2	+1.4	+1	+1.8

3.3 Supercell hazards

Overall, RMs exhibit higher average intensities of 5-min precipitation rate, and extend over larger areas for all hazards, consistent with their larger size compared to LMs (see Fig. 8 and 7). Specifically, the greater relative humidity in RMs is consistent with the higher intensity and area of precipitation (see Fig. 8b,g and Fig. 5f,g). As for hail size, LMs produce similarly sized
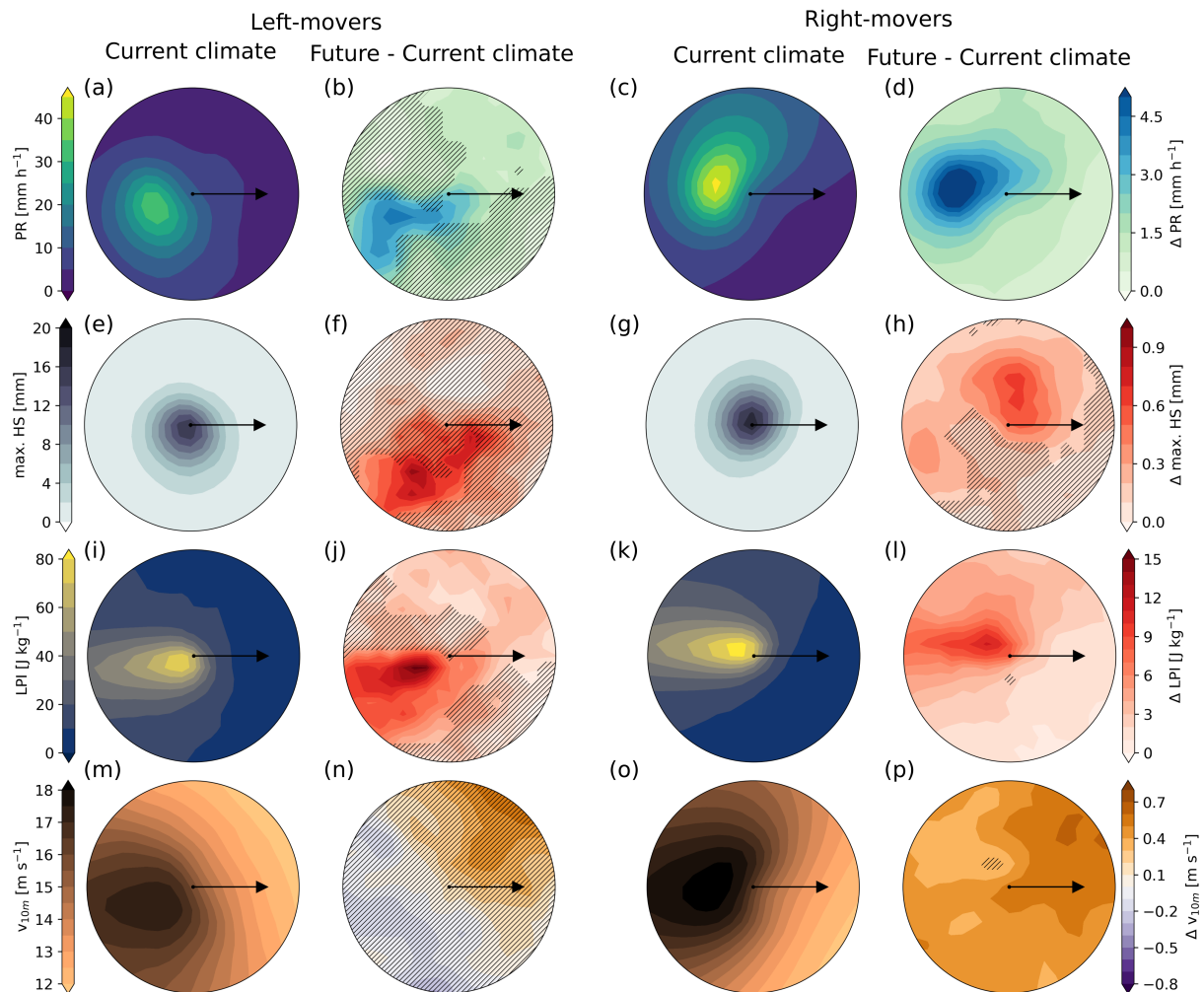
Figure 7. 5 min precipitation, 5 min max. hailsize, hourly max. lightning potential index and hourly max. 10m wind gust of LMs and RMs in the current climate and their climate change delta. Non-significant areas are hatched. The "cookies" (radius 20 km) show grid-point wise averages across all LM or RM cases and across all time steps.
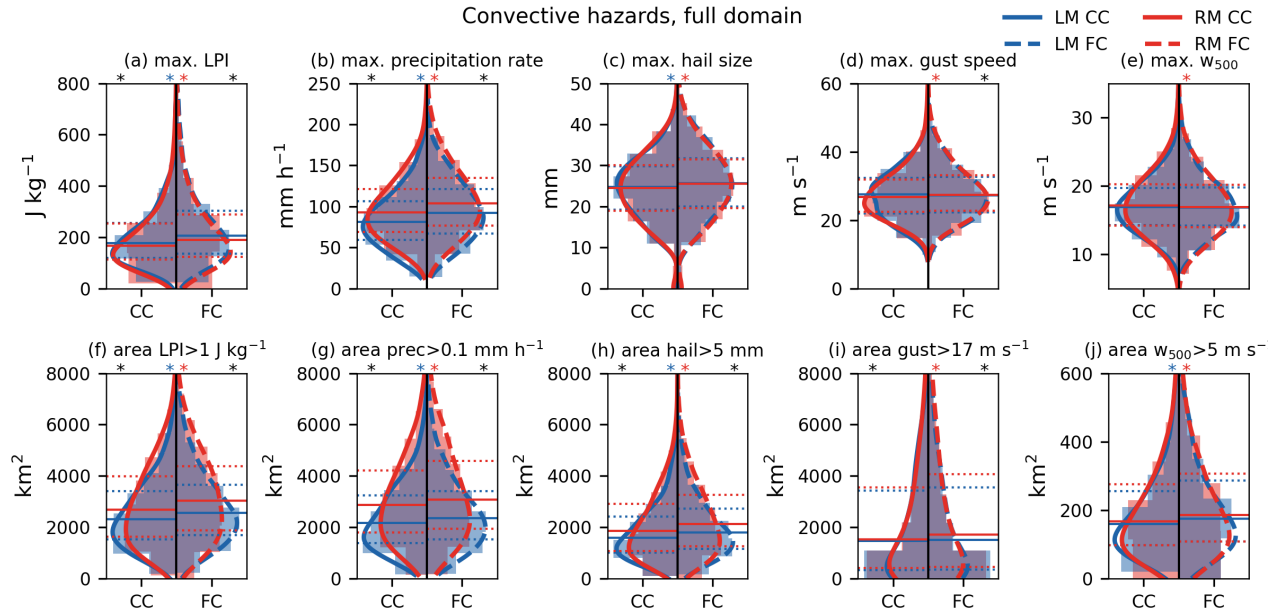
Figure 8. Density distributions of storm-associated maximum hazard intensities and hazard areas, interquartile range is indicated in dotted lines, the median with a solid line. The current climate (CC) is depicted on the left-hand side of each plot, the future climate (FC) on the right-hand side. Significant differences between the LMs are indicated with a blue asterisk, between the RMs with a red asterisk, between the current climate with a black asterisk on the left, and between the future climate with a black asterisk on the right.

hail as RMs, but over a smaller area (Fig. 8, second row). Notably, they lack the lower end of the max. hail size distribution, with smaller sizes being less common (Fig. 8c, LM distribution narrower at smallest sizes). Given the higher temperature, this

185   is consistent with the melting of hail (Gensini et al., 2024; Raupach et al., 2021; Dessens et al., 2015).

At the 3°C GWL, all hazard intensities increase significantly for both RMs and LMs, apart from LM wind gust intensity (Fig. 8, a-d). The hazard intensification contrasts with stable max. updraft speeds in both RM and LM (see Fig. 8e), however, updraft area increases significantly (Fig. 8j). The hazard intensity changes are larger for LMs, especially at the higher percentiles (not shown). Hence, despite LMs being a smaller subset of all supercell thunderstorms, their hazards are increasing more than those

190   of the total storm population. Hazard areas also increase consistently for both storm populations, apart from the surface gust area of LMs, which has no significant difference. Given the overall smaller size of LMs, the absolute change in hazard area is smaller than for RMs, but the relative change is of a similar magnitude.

The lack of significant change in surface wind gusts is surprising, as thermodynamic considerations suggest that with the

195   given change in environmental conditions, a more pronounced intensification should occur (expected ∼15%, Prein, 2023). However, the variable investigated depicts the hourly max. 10 m wind speed, and it is not at a 5-minute temporal resolution, as opposed to precipitation and hail metrics. Moreover, 10 m wind gusts are parametrized and not diagnosed directly in the model.

This may be responsible for part of this discrepancy. Another factor is the presence of considerable terrain over large parts of Europe, especially in the supercell occurrence hotspots of the Alpine region. Wind gust behavior in complex topography is

200 considerably more complicated and less straightforward to infer, as local channeling and damming effects nonlinearly affect the gust amplitude.

3.4 Regional comparison

To investigate the impact of local climates and their future changes on supercells, we use two subregions in the European domain: the Iberian Peninsula (IP) and the Northern Alps (NAL, see Figs. 9 and 10, regions defined in Fig. A1). The climate

205 of these two regions differs strongly between a dry, Mediterranean climate in IP and a moderate, strongly topographically influenced climate in NAL. The IP region is larger compared to NAL, with a moderate supercell occurrence (1420 mesocyclones and 20.8% LMs.) The NAL is a comparatively smaller region, however, it has a higher supercell occurrence with 447 detected mesocyclones in the current climate and a LM-ratio of 11.6%.

Comparing the pre-storm environmental conditions of the current climate in both regions (see Fig. 9), IP emerges as the region

210 where supercells form in hotter and drier conditions (Fig. 9 d,e,f); 850 hPa specific and relative humidity are considerably lower than in NAL (Fig. 9 e,f). This combination of hotter, but drier conditions results in comparable instability (Fig. 9a), with the range of the CAPE distribution being greater in NAL, reaching higher values in the upper percentiles. CIN is greater in IP, driven by the dryness (Fig. 9b). In the regional decomposition, the pattern of LM occurring in hotter and drier conditions also persists. In NAL we also find higher-CAPE conditions for LMs, but the dry conditions in IP compensate for the hotter

215 temperatures and lead to the same instability range for RMs and LMs. This further supports the hypothesis of LMs occurring a) closer to the ridge center in synoptically driven situations and b) preferentially during the convective peak in the day and year, when conditions are most optimal.

In line with the hotter and drier conditions, the distribution of maximum hail sizes in IP lacks the small hail sizes (Fig. 10c,

220 IP's distribution is narrower for small sizes than NAL's), consistent with melting signatures. However, upwards of the median, the percentiles are distributed very similarly to NAL (Fig. 10c,h). IP also has lower precipitation intensities that decrease for LMs in the future climate but increase for RMs (Fig. 10b,g). This suggests that for these storms, while the warmer air could carry more moisture, there is not enough specific humidity available to sustain higher precipitation rates or greater precipitation areas. The increase in RM precipitation rates may result from the larger shear, which increases storm area and organization,

225 RH, and updraft area and may overcompensate for the slight decrease in updraft strength (e.g., Mulholland et al., 2024; Nielsen and Schumacher, 2020, 2018). In both regions, LMs reach higher lightning activity, but in a smaller area than RMs (Fig. 10a,f). Lightning activity in NAL is slightly greater than in IP, possibly related to the greater moisture content. IP has a greater potential for wind gusts in area and speed (Fig. 10d,i). Strong gusts are more likely in drier conditions that can initiate and accelerate downbursts through evaporative cooling (Díaz-Fernández et al., 2025; Romanic et al., 2022; Srivastava, 1985).

230 Overall, within these sub-regions, the hazard intensities between LMs and RMs differ more than between the climate scenarios.
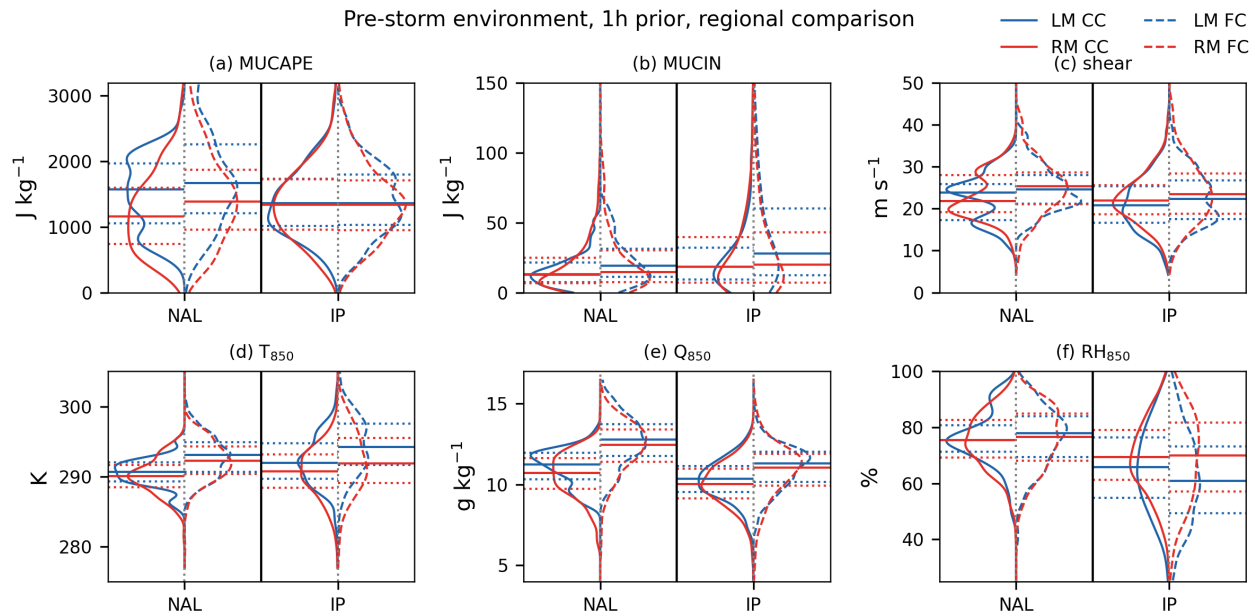
Figure 9. Density distributions of pre-storm environment, interquartile range is indicated in dotted lines, the median with a solid line. The current climate (CC) is depicted on the left-hand side of each plot, the future climate (FC) on the right-hand side. The two regions are depicted in the respective halves of the panels.

Moreover, LMs can have equal or higher intensity hazards, but tend to have them in a smaller area, as their size is overall smaller.

4 Summary and Discussion

In the km-scale climate model data, our methods identified ∼8200 RMs and ∼1200 LMs in the current climate. We find an 8% increase of RMs and 14% increase of LMs in a +3°C climate. We emphasize that while the fraction of RMs is 87% of the total supercell population, we are likely undercounting the number of LMs due to their short-lived and transient nature (Zeeb et al., under review; Van Den Broeke et al., under review; Wade and Parker, 2021; Sherburn et al., 2016; Sherburn and Parker, 2014). In the simulated data, both storm types show a realistic, albeit smooth, morphology with distinct right- and left-leaning features and characteristic motion deviations from the mean flow with correspondingly curved hodographs. The fraction of LMs increases marginally (+1%) in the warmer climate, however the relative increase of LMs (+21%) is approximately twice that of RMs (+8%).

For both RM and LM hodographs, modeled storm motion deviates less from the hodograph than Bunkers' storm motion would suggest. As suggested by Tonn et al. (2023), a reduction of the offset may be warranted in Europe, in addition to having
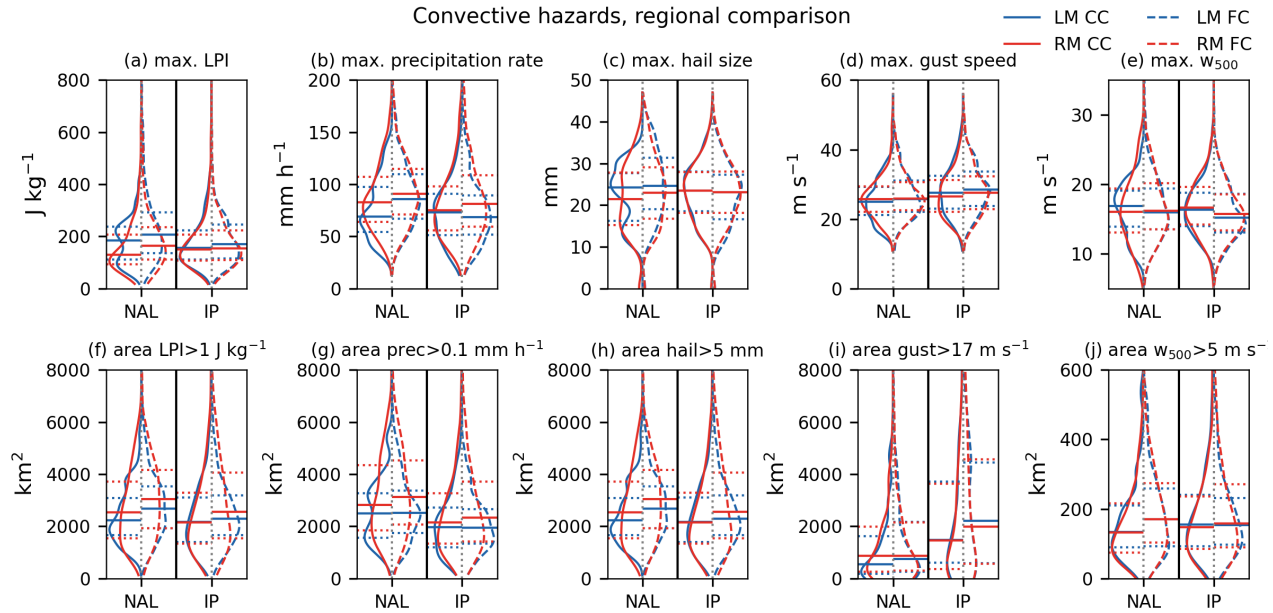
Figure 10. Density distributions of storm-associated maximum hazard intensities and hazard areas, interquartile range is indicated in dotted lines, the median with a solid line. The current climate (CC) is depicted on the left-hand side of each plot, the future climate (FC) on the right-hand side. The two regions are depicted in the respective halves of the panels.

a smaller offset for LMs than RMs (Bunkers et al., 2024). Our analyses propose separate offsets of C_{RM} = 5 m s^{-1} and C_{LM} = 1 m s^{-1}. The hodographs overall show that shear is largely concentrated at the 850-700 hPa level, while the near-surface change in wind speed is very gradual (also found in Taszarek et al., 2020; Peyraud, 2013; Houze et al., 1993), contrasting the typical supercell environments of the Great Plains, which tend to have large amounts of shear in the first km (e.g., Davenport, 2021).

The identified generally northeasterly track of supercells is well-supported by literature showing SW flow during severe convective outbreaks in Europe (Feldmann et al., 2025b, 2021; Mohr et al., 2020; Wapler and James, 2014). The future shift to more northerly tracks may be owed to the spatial shift towards NE Europe (Feldmann et al., 2025a), as synoptic drivers have distinct regional characteristics throughout Europe (Feldmann et al., 2025b; Ghasemifard et al., 2024).

Furthermore, the analysis of hodographs revealed an overall backing hodograph for LMs, which is synoptically less likely to occur in the overall convectively favorable prefrontal zone, where warm air advection and veering generally dominate (van Delden, 1998). In combination with the higher mean sea level pressure for LMs, they appear to occur further away from an approaching trough and closer to the center of the downstream ridge, where veering is less pronounced and a backing hodograph has a higher likelihood. Additionally, our results show that LMs occur at higher temperatures and greater instability, and are more likely around the convective peak of the day and season, which has also been found in observational studies targeting the United States (Zeeb et al., under review; Van Den Broeke et al., under review; Homeyer et al., 2025). The higher temperatures

15

further suggest the closer location of LMs to the ridge axis, as conditions near the ridge center are increasingly hotter and drier. These conditions often result in less favorable convective conditions, potentially causing the lower percentage of LMs in the overall supercell population.

In comparison to RMs in the current climate, the future climate, as well as LMs in all climates have increased instability and
265 increased convective inhibition. The steeper moist adiabat at higher temperatures not only represents a greater potential of the atmosphere to hold moisture at warmer temperatures, in accordance with Clausius-Clapeyron, but also the change in condensation rate (Emanuel, 2023). When cooling down a saturated parcel at warmer temperatures, it will condense more moisture per °C of cooling than an absolutely colder parcel. This leads to a simultaneous increase of CAPE and CIN, when RH remains approximately unchanged.

270 Analyses of surface hazards show that even though LMs are the minority across the storm population, they are associated with considerable hazard intensities and their hazards increase stronger than those of RMs in the warmer climate. Nonetheless, RMs are the more intense storm type overall. Additionally, in combination with the lower fractional percentage of LMs, LMs remain poorly documented in the European context, and few studies provide detailed analyses of their structure, environments, or hazards (e.g., Houze et al., 1993). Consequently, some of our findings cannot be directly compared to previous literature,
275 highlighting the need for further research on this storm type. In the limited previous literature, LMs have been described as prolific hail producers (Zeeb et al., under review; Nelson, 2024; Houze et al., 1993). The similar hail size distribution to RMs, as well as their marked hail size increase at 3°C, support this notion. LMs have a smaller fraction of non-hailing storms, and since LMs occur in higher temperatures and greater instability, these may result in a more potent hail environment, possibly skewing the hail size distribution towards larger sizes as small hail stones melt disproportionately more in the warmer con-
280 ditions (effects of melting also discussed in Gensini et al., 2024; Raupach et al., 2021; Dessens et al., 2015). Additionally, LMs show equally high lightning and gust magnitudes as RMs, stressing the importance of not neglecting this fraction of the storm population. LMs are ∼35% smaller and thus their hazards are concentrated into a smaller area. In combination with their shorter and more transient lifecycles, this makes for a very volatile storm type that has the potential to be very damaging in a comparatively small area and short amount of time. While the total damages are spatially more confined than with RMs, the
285 local impacts can be just as devastating, emphasizing the need for accurate warnings and forecasts.

In the future climate, the median updraft strength across all supercells slightly decreases, while the updraft area increases slightly. As such, the overall increases in surface hazards (e.g., precipitation rates, hailfall, wind gusts) for both RMs and LMs can be explained by the changes in the storm environment, whereas the changes in hazard area may be related to the increase in
290 updraft width, allowing greater moisture transport for precipitation. Precipitation intensity and area increase in agreement with Clausius-Clapeyron scaling (Estermann et al., 2025; Ban et al., 2020, 2015). Zeeb et al. (2024) shows a similar increase of the precipitation intensities in RM supercells in the United States. Precipitation changes may also be modulated by the increase in low-level moisture, temperature, CAPE, and shear, leading to potentially stronger storms and subsequent intensification of precipitation production (e.g., Mulholland et al., 2024; Nielsen and Schumacher, 2020, 2018). While surface wind gusts intensify
295 by ∼5% in RMs, the increase is smaller than expected based on the environmental changes, which suggest a ∼15% increase

(Prein, 2023). Possible limitations here may be that wind gusts are an hourly accumulated maximum, instead of a 5-minute output variable, as well as the influence of complex topography on surface wind phenomena and the limitations of the gust parametrization.

300   Regional climate regimes introduce heterogeneity into the dominant pre-storm conditions and subsequent hazard properties, but overall show features consistent with the mean climate analyses and existing literature. Comparing the Iberian Peninsula (IP) and Northern Alps (NAL) contrasts a hot and dry climate with a negative supercell frequency trend and a cooler, moister, and mountainous region with an increasing supercell frequency. At the 3°C warming level, IP experiences a significant decrease in overall supercell occurrence of 30%, whereas activity in NAL increases significantly by 50%, with their LM fractions

305   remaining unchanged (Feldmann et al., 2025a). Overall, these changes in supercell frequency are caused by changes in the frequency of unstable days. Specifically, the increasingly dry summers of IP reduce the number of days, where CAPE exceeds 100 J kg^{-1} (Thurnherr et al., 2025; Feldmann et al., 2025a). IP has no further reduction in relative humidity for RMs in the pre-storm environment, as specific humidity rises accordingly with the local warming. This is a sign that IP's storms are near the limit of how dry conditions can be, while still supporting deep moist convection; median relative humidity values around

310   60-70% for LMs are comparatively low (Feldmann et al., 2025b). NAL's climate change signal, however, is closer to the domain mean, with CAPE and CIN increasing alongside low-level temperature and specific humidity; low-level relative humidity remains stable for RMs. These increases result in more frequent unstable days (Thurnherr et al., 2025; Feldmann et al., 2025a), therefore significantly increasing the supercell occurrence in NAL.

The regional comparison highlights IP as a drier region than NAL, with comparable instability values (also found in observa-

315   tions/reanalysis in Feldmann et al., 2023; Calvo-Sancho et al., 2022). The drier environment in IP reduces the hailfall area, but increases gust area. Previous studies have shown downburst-favorable environments for IP (Díaz-Fernández et al., 2025; Calvo-Sancho et al., 2022; Romanic et al., 2022). The complex topography and varied environments in NAL produce a wider range of instability conditions supporting supercell development for both RMs and LMs (Feldmann et al., 2024). The more humid conditions also make NAL a region more prone to larger hail-, precipitation-, and lightning areas per storm (Estermann et al.,

320   2025; Cui et al., 2023; Feldmann et al., 2023; Nielsen and Schumacher, 2020; Ban et al., 2020; Nielsen and Schumacher, 2018).

Some inherent limitations of the work here are owed to the limitations of the climate simulation. A 2.2 km horizontal resolution is still on the coarse end for representing supercellular convection (Prein et al., 2025; Weisman et al., 2023); however, it is currently the highest resolution available, especially for the spatio-temporal dimensions of the dataset. Feldmann et al.

325   (2025a) show that this resolution is sufficient to capture the spatio-temporal distribution of supercells with mesocyclones of at least 5 km diameter. Nonetheless, smaller and shorter-lived storms are missed by the tracking, affecting LMs disproportionately, provided their smaller and more transient nature. While observational references for LMs are strongly limited, we assume that the identified proportion of 25% LMs in Tonn et al. (2023) is more realistic than the <15% identified here.

Likewise, the PGW approach here constitutes a single realization of a 3°C warming scenario. While the chosen driving climate

330   model member is close to the ensemble mean with respect to summer precipitation (Thurnherr et al., 2025), this method does

not provide uncertainty information on the range of general possible conditions at a 3°C GWL. Presumably, this uncertainty affects overall storm frequency changes more than the environmental changes when a storm is already present in the model.

5   Conclusions

The analysis of the regional climate data has allowed us to fundamentally compare right- (RM) and left-moving (LM) supercells
335   from a climatological perspective. Revisiting the questions raised in the beginning, we can summarize as follows:

1. **Comparison of structure, environments, and intensity:** LMs constitute a minority (13%) fraction of storms, but can achieve similar hazard intensities as RMs. They are smaller and their averaged curvature is less pronounced than the right-leaning curvature of the RMs (see Fig. 11 for a graphical summary). LMs occur in a narrow range of environmental conditions, on average in higher temperatures and in less stable conditions, with a weakly backing hodograph, found in
340   higher-mean sea level pressure locations with smaller horizontal pressure gradients.

2. **Comparison of climate change signal:** The instability and hazards of LMs increase more than those of RMs at the 3°C GWL. Despite the frequency split remaining stable in the model, the hazard intensity increases disproportionately for LMs. For both storm types, the updraft strength remains stable, while the updraft area increases slightly. Hazard intensities and areas increase in future.

345   3. **The role of regional heterogeneity:** The comparison of two different climate regimes—one with a drier and hotter climate and the other with a moister and cooler climate—leads to different supercell frequency changes in the future, showing that key environmental characteristics persist across diverse climate regimes. Regionally, LMs occur in warmer and less stable conditions than RMs. Overall, the differences between regional climates are generally greater than the differences between LMs and RMs, whereas the differences between LMs and RMs are greater than the differences
350   between the climate scenarios.

Overall, supercell thunderstorms in Europe are expected to increase in both occurrence and hazard intensity, as their environments grow more potent, with increases in both CAPE and deep-layer shear, supported by increases in specific humidity. The intensity increase is largely decoupled from regional frequency changes. Near-storm environments are preconditioned by the presence of a storm, and while they still lean towards their background climate, certain conditions are always filled, such
355   as moisture availability, instability, and deep-layer shear.

Fundamentally understanding the differences between RMs' and LMs' hazard potential and environments allows for the development of better warning and forecasting tools. The majority of forecasting parameters, such as the supercell composite parameter, are mostly tuned to the occurrence of severe RMs (Zeeb et al., under review). Given the high hazard potential of
360   LMs and their disproportionate intensification with climate change, better forecasting metrics are essential. Especially in regions like the Alpine region, where the frequency increase is considerable (Feldmann et al., 2025a) and the intensity of LMs
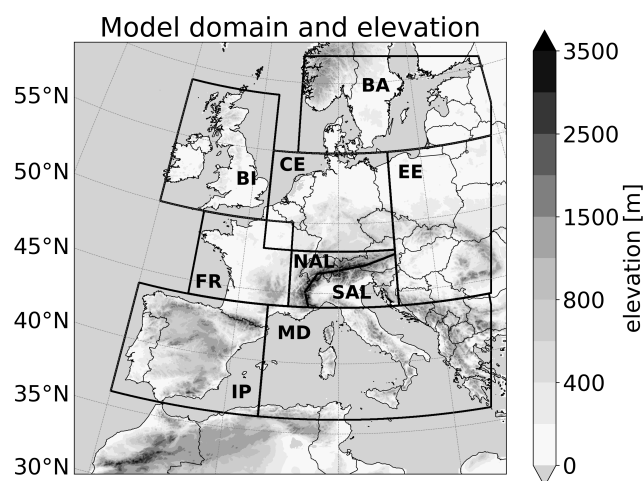
18
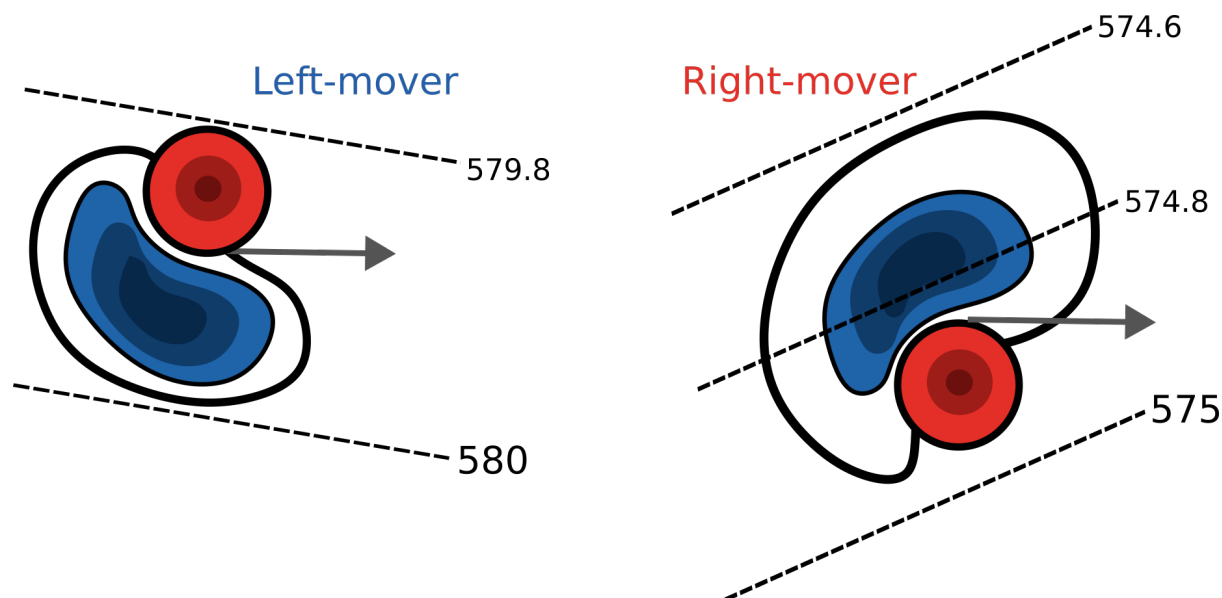
Figure 11. Schematic of supercell structures: black outline — precipitation contour, red area — updraft, blue area — downdraft, black dashed lines — isohypses (dam), gray arrow — storm motion. Structural differences between LM and RM: smaller storm area, similar strength up- and downdrafts, less deviant motion for LMs, lesser gradient of geopotential height, and greater geopotential height. Features are exaggerated and not true to scale.

rivals RMs, accurate projections of severe weather potential are a key requirement for climate adaptation.

Given the scarcity of literature on LMs, both further observational and modeling studies are essential to fully characterize the processes differentiating them from RMs. LMs are not simply a mirror of RMs, but rather a distinct storm type with unique morphology, environmental conditions, and hazard potential. More broadly, the response of supercells to climate change remains subject to considerable uncertainty. Longer observational records and high-resolution ensemble simulations will be key to constraining future risks and improving preparedness.

Code and data availability. The code used to extract the storm environment is available at https://doi.org/10.5281/zenodo.14631622. Storm tracks are available at https://doi.org/10.5281/zenodo.13378057. The code used for further analyses and visualization of the data is available at https://github.com/feldmann-m/SC_left_right. The extracted cookies at 0 and 1 hours lag will be made available during the review process.

Figure A1. Model domain and elevation, including sub-regions

Appendix A: Model domain

References

Ashley, W. S., Haberlie, A. M., and Gensini, V. A.: The Future of Supercells in the United States, Bulletin of the American Meteorological Society, 104, E1–E21, https://doi.org/10.1175/BAMS-D-22-0027.1, publisher: American Meteorological Society Section: Bulletin of the American Meteorological Society, 2023.

Ban, N., Schmidli, J., and Schär, C.: Heavy precipitation in a changing climate: Does short-term summer precipitation increase faster?, Geophysical Research Letters, 42, 1165–1172, https://doi.org/10.1002/2014GL062588, _eprint: https://onlinelibrary.wiley.com/doi/pdf/10.1002/2014GL062588, 2015.

Ban, N., Rajczak, J., Schmidli, J., and Schär, C.: Analysis of Alpine precipitation extremes using generalized extreme value theory in convection-resolving climate simulations, Climate Dynamics, 55, 61–75, https://doi.org/10.1007/s00382-018-4339-4, 2020.

Barras, H., Hering, A., Martynov, A., Noti, P.-A., Germann, U., and Martius, O.: Experiences with >50,000 Crowdsourced Hail Reports in Switzerland, Bulletin of the American Meteorological Society, 100, 1429–1440, https://doi.org/10.1175/BAMS-D-18-0090.1, publisher: American Meteorological Society Section: Bulletin of the American Meteorological Society, 2019.

Battaglioli, F., Groenemeijer, P., Púčik, T., Taszarek, M., Ulbrich, U., and Rust, H.: Modeled Multidecadal Trends of Lightning and (Very) Large Hail in Europe and North America (1950–2021), Journal of Applied Meteorology and Climatology, 62, 1627–1653, https://doi.org/10.1175/JAMC-D-22-0195.1, publisher: American Meteorological Society Section: Journal of Applied Meteorology and Climatology, 2023.

Benjamini, Y. and Hochberg, Y.: Controlling the False Discovery Rate: A Practical and Powerful Approach to Multiple Testing, Journal of the Royal Statistical Society: Series B (Methodological), 57, 289–300, https://doi.org/10.1111/j.2517-6161.1995.tb02031.x, _eprint: https://onlinelibrary.wiley.com/doi/pdf/10.1111/j.2517-6161.1995.tb02031.x, 1995.

Brennan, K. P., Sprenger, M., Walser, A., Arpagaus, M., and Wernli, H.: An object-based and Lagrangian view on an intense hailstorm day in Switzerland as represented in COSMO-1E ensemble hindcast simulations, EGUsphere, pp. 1–31, https://doi.org/10.5194/egusphere-2024-2148, publisher: Copernicus GmbH, 2024.

Brennan, K. P., Thurnherr, I., Sprenger, M., and Wernli, H.: Insights from hailstorm track analysis in European climate change simulations, Nat. Hazards Earth Syst. Sci., p. 3693–3712, https://doi.org/10.5194/nhess-25-3693-2025, publisher: Copernicus GmbH, 2025.

Brogli, R., Heim, C., Mensch, J., Sørland, S. L., and Schär, C.: The pseudo-global-warming (PGW) approach: methodology, software package PGW4ERA5 v1.1, validation, and sensitivity analyses, Geoscientific Model Development, 16, 907–926, https://doi.org/10.5194/gmd-16-907-2023, publisher: Copernicus GmbH, 2023.

Bunkers, M. J.: Vertical Wind Shear Associated with Left-Moving Supercells, Weather and Forecasting, 17, 845–855, https://doi.org/10.1175/1520-0434(2002)017<0845:VWSAWL>2.0.CO;2, publisher: American Meteorological Society Section: Weather and Forecasting, 2002.

Bunkers, M. J., Klimowski, B. A., Zeitler, J. W., Thompson, R. L., and Weisman, M. L.: Predicting Supercell Motion Using a New Hodograph Technique, Weather and Forecasting, 15, 61 – 79, https://doi.org/10.1175/1520-0434(2000)015<0061:PSMUAN>2.0.CO;2, place: Boston MA, USA Publisher: American Meteorological Society, 2000.

Bunkers, M. J., Broeke, M. S. V. D., and Allen, J. T.: An Update for Predicting Left-Moving Supercell Motion, Weather and Forecasting, 39, 1777–1794, https://doi.org/10.1175/WAF-D-24-0028.1, publisher: American Meteorological Society Section: Weather and Forecasting, 2024.

Calvo-Sancho, C., Díaz-Fernández, J., Martín, Y., Bolgiani, P., Sastre, M., González-Alemán, J. J., Santos-Muñoz, D., Farrán, J. I., and Martín, M. L.: Supercell convective environments in Spain based on ERA5: hail and non-hail differences, Weather and Climate Dynamics, 3, 1021–1036, https://doi.org/10.5194/wcd-3-1021-2022, publisher: Copernicus GmbH, 2022.

Cui, R., Ban, N., Demory, M.-E., and Schär, C.: Exploring hail and lightning diagnostics over the Alpine-Adriatic region in a km-scale
425   climate model, Weather and Climate Dynamics Discussions, 2023, 1–31, https://doi.org/10.5194/wcd-2023-11, 2023.

Cui, R., Thurnherr, I., Velasquez, P., Brennan, K. P., Leclair, M., Mazzoleni, A., Schmid, T., Wernli, H., and Schär, C.: A European Hail and Lightning Climatology From an 11-Year Kilometer-Scale Regional Climate Simulation, Journal of Geophysical Research: Atmospheres, 130, e2024JD042 828, https://doi.org/10.1029/2024JD042828, _eprint: https://agupubs.onlinelibrary.wiley.com/doi/pdf/10.1029/2024JD042828, 2025.

430   Davenport, C. E.: Environmental Evolution of Long-Lived Supercell Thunderstorms in the Great Plains, Weather and Forecasting, 36, 2187–2209, https://doi.org/10.1175/WAF-D-21-0042.1, publisher: American Meteorological Society Section: Weather and Forecasting, 2021.

Davies-Jones, R.: Streamwise Vorticity: The Origin of Updraft Rotation in Supercell Storms, Journal of Atmospheric Sciences, 41, 2991 – 3006, https://doi.org/https://doi.org/10.1175/1520-0469(1984)041<2991:SVTOOU>2.0.CO;2, place: Boston MA, USA Publisher: American Meteorological Society, 1984.

435   Davies-Jones, R.: Linear and Nonlinear Propagation of Supercell Storms, Journal of the Atmospheric Sciences, 59, 3178–3205, https://doi.org/10.1175/1520-0469(2003)059<3178:LANPOS>2.0.CO;2, publisher: American Meteorological Society Section: Journal of the Atmospheric Sciences, 2002.

Davies-Jones, R.: A review of supercell and tornado dynamics, Atmospheric Research, 158-159, 274–291, https://doi.org/10.1016/j.atmosres.2014.04.007, 2015.

440   Dessens, J., Berthet, C., and Sanchez, J. L.: Change in hailstone size distributions with an increase in the melting level height, Atmospheric Research, 158-159, 245–253, https://doi.org/10.1016/j.atmosres.2014.07.004, 2015.

Díaz-Fernández, J., Calvo-Sancho, C., Bolgiani, P., Sastre, M., López-Reyes, M., Fernández-González, S., and Martín, M. L.: Effect of complex orography on numerical simulations of a downburst event in Spain, Atmospheric Research, 314, 107 821, https://doi.org/10.1016/j.atmosres.2024.107821, 2025.

445   Emanuel, K.: On the Physics of High CAPE, Journal of the Atmospheric Sciences, 80, 2669–2683, https://doi.org/10.1175/JAS-D-23-0060.1, publisher: American Meteorological Society Section: Journal of the Atmospheric Sciences, 2023.

Estermann, R., Rajczak, J., Velasquez, P., Lorenz, R., and Schär, C.: Projections of Heavy Precipitation Characteristics Over the Greater Alpine Region Using a Kilometer–Scale Climate Model Ensemble, Journal of Geophysical Research: Atmospheres, 130, e2024JD040 901, https://doi.org/https://doi.org/10.1029/2024JD040901, e2024JD040901 2024JD040901, 2025.

450   Feldmann, M., Germann, U., Gabella, M., and Berne, A.: A characterisation of Alpine mesocyclone occurrence, Weather and Climate Dynamics, 2, 1225–1244, https://doi.org/10.5194/wcd-2-1225-2021, publisher: Copernicus GmbH, 2021.

Feldmann, M., Hering, A., Gabella, M., and Berne, A.: Hailstorms and rainstorms versus supercells—a regional analysis of convective storm types in the Alpine region, npj Climate and Atmospheric Science, 6, 1–11, https://doi.org/10.1038/s41612-023-00352-z, number: 1 Publisher: Nature Publishing Group, 2023.

455   Feldmann, M., Rotunno, R., Germann, U., and Berne, A.: Supercell Thunderstorms in Complex Topography—How Mountain Valleys with Lakes Can Increase Occurrence Frequency, Monthly Weather Review, 152, 471–489, https://doi.org/10.1175/MWR-D-22-0350.1, publisher: American Meteorological Society Section: Monthly Weather Review, 2024.

Feldmann, M., Blanc, M., Brennan, K. P., Thurnherr, I., Velasquez, P., Martius, O., and Schär, C.: European supercell thunderstorms—A prevalent current threat and an increasing future hazard, Science Advances, 11, eadx0513, https://doi.org/10.1126/sciadv.adx0513, publisher: American Association for the Advancement of Science, 2025a.

460 Feldmann, M., Domeisen, D. I. V., and Martius, O.: A pan-European analysis of large-scale drivers of severe convective outbreaks, EGUsphere, pp. 1–24, https://doi.org/10.5194/egusphere-2025-2296, publisher: Copernicus GmbH, 2025b.

Gensini, V. A., Ashley, W. S., Michaelis, A. C., Haberlie, A. M., Goodin, J., and Wallace, B. C.: Hailstone size dichotomy in a warming climate, 7, 185, https://doi.org/10.1038/s41612-024-00728-9, 2024.

465 Germann, U., Boscacci, M., Clementi, L., Gabella, M., Hering, A., Sartori, M., Sideris, I. V., and Calpini, B.: Weather Radar in Complex Orography, Remote Sensing, 14, 503, https://doi.org/10.3390/rs14030503, number: 3 Publisher: Multidisciplinary Digital Publishing Institute, 2022.

Ghasemifard, H., Groenemeijer, P., Battaglioli, F., and Púčik, T.: Do changing circulation types raise the frequency of summertime thunderstorms and large hail in Europe?, Environmental Research: Climate, 3, 015 008, https://doi.org/10.1088/2752-5295/ad22ec, publisher: IOP Publishing, 2024.

470 Hersbach, H., Bell, B., Berrisford, P., Hirahara, S., Horányi, A., Muñoz-Sabater, J., Nicolas, J., Peubey, C., Radu, R., Schepers, D., Simmons, A., Soci, C., Abdalla, S., Abellan, X., Balsamo, G., Bechtold, P., Biavati, G., Bidlot, J., Bonavita, M., De Chiara, G., Dahlgren, P., Dee, D., Diamantakis, M., Dragani, R., Flemming, J., Forbes, R., Fuentes, M., Geer, A., Haimberger, L., Healy, S., Hogan, R. J., Hólm, E., Janisková, M., Keeley, S., Laloyaux, P., Lopez, P., Lupu, C., Radnoti, G., de Rosnay, P., Rozum, I., Vamborg, F., Villaume, S., and Thépaut, J.-N.: The ERA5 global reanalysis, Quarterly Journal of the Royal Meteorological Society, 146, 1999–2049, https://doi.org/https://doi.org/10.1002/qj.3803, _eprint: https://rmets.onlinelibrary.wiley.com/doi/pdf/10.1002/qj.3803, 2020.

Homeyer, C. R., Bunkers, M. J., Allen, J. T., and Murphy, A. M.: United States Supercell Storms and Their Severity: A 14-yr Radar-Based Climatology, Journal of Applied Meteorology and Climatology, -1, https://doi.org/10.1175/JAMC-D-24-0185.1, publisher: American Meteorological Society Section: Journal of Applied Meteorology and Climatology, 2025.

480 Houze, R. A., Schmid, W., Fovell, R. G., and Schiesser, H.-H.: Hailstorms in Switzerland: Left Movers, Right Movers, and False Hooks, Monthly Weather Review, 121, 3345–3370, https://doi.org/10.1175/1520-0493(1993)121<3345:HISLMR>2.0.CO;2, publisher: American Meteorological Society Section: Monthly Weather Review, 1993.

Markowski, P. and Richardson, Y.: Mesoscale Meteorology in Midlatitudes, Wiley-Blackwell, https://doi.org/10.1002/9780470682104, 2010.

McKnight, P. E. and Najab, J.: Mann-Whitney U Test, in: The Corsini Encyclopedia of Psychology, pp. 1–1, John Wiley & Sons, Ltd, https://doi.org/10.1002/9780470479216.corpsy0524, _eprint: https://onlinelibrary.wiley.com/doi/pdf/10.1002/9780470479216.corpsy0524, 2010.

Mohr, S., Wilhelm, J., Wandel, J., Kunz, M., Portmann, R., Punge, H. J., Schmidberger, M., Quinting, J. F., and Grams, C. M.: The role of large-scale dynamics in an exceptional sequence of severe thunderstorms in Europe May–June 2018, Weather and Climate Dynamics, 1, 325–348, https://doi.org/10.5194/wcd-1-325-2020, 2020.

490 Mulholland, J. P., Nowotarski, C. J., Peters, J. M., Morrison, H., and Nielsen, E. R.: How Does Vertical Wind Shear Influence Updraft Characteristics and Hydrometeor Distributions in Supercell Thunderstorms?, Monthly Weather Review, 152, 1663–1687, https://doi.org/10.1175/MWR-D-23-0166.1, 2024.

Nelson, R.: Polarimetric Radar Signatures in Significant Severe Left-moving Supercells, Department of Earth and Atmospheric Sciences: Dissertations, Theses, and Student Research, https://digitalcommons.unl.edu/geoscidiss/158, 2024.

495 Nielsen, E. R. and Schumacher, R. S.: Dynamical Insights into Extreme Short-Term Precipitation Associated with Supercells and Mesovortices, Journal of the Atmospheric Sciences, 75, 2983–3009, https://doi.org/10.1175/JAS-D-17-0385.1, 2018.

Nielsen, E. R. and Schumacher, R. S.: Dynamical Mechanisms Supporting Extreme Rainfall Accumulations in the Houston "Tax Day" 2016 Flood, Monthly Weather Review, 148, 83–109, https://doi.org/10.1175/MWR-D-19-0206.1, 2020.

Nisi, L., Hering, A., Germann, U., and Martius, O.: A 15-year hail streak climatology for the Alpine region,
500 Quarterly Journal of the Royal Meteorological Society, 144, 1429–1449, https://doi.org/10.1002/qj.3286, _eprint: https://onlinelibrary.wiley.com/doi/pdf/10.1002/qj.3286, 2018.

Peyraud, L.: Analysis of the 18 July 2005 Tornadic Supercell over the Lake Geneva Region, Weather and Forecasting, 28, 1524–1551, https://doi.org/10.1175/waf-d-13-00022.1, 2013.

Prein, A. F.: Thunderstorm straight line winds intensify with climate change, Nature Climate Change, 13, 1353–1359,
505 https://doi.org/10.1038/s41558-023-01852-9, number: 12 Publisher: Nature Publishing Group, 2023.

Prein, A. F., Wang, D., Ge, M., Ramos Valle, A., and Chasteen, M. B.: Resolving Mesoscale Convective Systems: Grid Spacing Sensitivity in the Tropics and Midlatitudes, Journal of Geophysical Research: Atmospheres, 130, e2024JD042 530, https://doi.org/10.1029/2024JD042530, _eprint: https://agupubs.onlinelibrary.wiley.com/doi/pdf/10.1029/2024JD042530, 2025.

Pîrloagă, R., Ene, D., and Antonescu, B.: Population Bias on Tornado Reports in Europe, Applied Sciences, 11, 11 485,
510 https://doi.org/10.3390/app112311485, publisher: Multidisciplinary Digital Publishing Institute, 2021.

Raupach, T. H., Martius, O., Allen, J. T., Kunz, M., Lasher-Trapp, S., Mohr, S., Rasmussen, K. L., Trapp, R. J., and Zhang, Q.: The effects of climate change on hailstorms, Nature Reviews Earth & Environment, 2, 213–226, https://doi.org/10.1038/s43017-020-00133-9, number: 3 Publisher: Nature Publishing Group, 2021.

Romanic, D., Taszarek, M., and Brooks, H.: Convective environments leading to microburst, macroburst and downburst events across the
515 United States, Weather and Climate Extremes, 37, 100 474, https://doi.org/10.1016/j.wace.2022.100474, 2022.

Saltikoff, E., Haase, G., Delobbe, L., Gaussiat, N., Martet, M., Idziorek, D., Leijnse, H., Novák, P., Lukach, M., and Stephan, K.: OPERA the Radar Project, Atmosphere, 10, 320, https://doi.org/10.3390/atmos10060320, publisher: Multidisciplinary Digital Publishing Institute, 2019.

Sherburn, K. D. and Parker, M. D.: Climatology and Ingredients of Significant Severe Convection in High-Shear, Low-CAPE Environments,
520 Weather and Forecasting, 29, 854–877, https://doi.org/10.1175/WAF-D-13-00041.1, publisher: American Meteorological Society Section: Weather and Forecasting, 2014.

Sherburn, K. D., Parker, M. D., King, J. R., and Lackmann, G. M.: Composite Environments of Severe and Nonsevere High-Shear, Low-CAPE Convective Events, Weather and Forecasting, 31, 1899–1927, https://doi.org/10.1175/WAF-D-16-0086.1, publisher: American Meteorological Society Section: Weather and Forecasting, 2016.

525 Srivastava, R. C.: A Simple Model of Evaporatively Driven Downdraft: Application to Microburst Downdraft, Journal of Atmospheric Sciences, 42, 1004–1023, https://doi.org/10.1175/1520-0469(1985)042<1004:ASMOED>2.0.CO;2, 1985.

Taszarek, M., Kendzierski, S., and Pilguj, N.: Hazardous weather affecting European airports: Climatological estimates of situations with limited visibility, thunderstorm, low-level wind shear and snowfall from ERA5, Weather and Climate Extremes, 28, 100 243, https://doi.org/10.1016/j.wace.2020.100243, 2020.

530 Taszarek, M., Allen, J. T., Brooks, H. E., Pilguj, N., and Czernecki, B.: Differing Trends in United States and European Severe Thunderstorm Environments in a Warming Climate, Bulletin of the American Meteorological Society, 102, E296–E322, https://doi.org/10.1175/BAMS-D-20-0004.1, publisher: American Meteorological Society Section: Bulletin of the American Meteorological Society, 2021.

Thurnherr, I., Cui, R., Velasquez, P., Wernli, H., and Schär, C.: The effect of 3°C global warming on hail over Europe, Geophysical Research Letters, https://www.authorea.com/users/758365/articles/1262765-the-effect-of-3-c-global-warming-on-hail-over-europe?commit=b0bd3757c594bd6ade6ad45c4bb09fc5c7cb48cf, 2025.

Tonn, M., Wilhelm, J., and Kunz, M.: Evaluating Bunkers' storm motion of hail-producing supercells and their storm-relative helicity in Germany, Meteorologische Zeitschrift, pp. 229–243, https://doi.org/10.1127/metz/2023/1165, publisher: Schweizerbart'sche Verlagsbuchhandlung, 2023.

van Delden, A.: The synoptic setting of a thundery low and associated prefrontal squall line in western Europe, Meteorology and Atmospheric Physics, 65, 113–131, https://doi.org/10.1007/BF01030272, 1998.

Van Den Broeke, M., Van Den Broeke, C., and Schweigert, B.: Spatiotemporal Characteristics of Anticyclonic Supercells in the Contiguous United States, J. Appl. Meteor. Climatol., in review, under review.

Ventura, V., Paciorek, C. J., and Risbey, J. S.: Controlling the Proportion of Falsely Rejected Hypotheses when Conducting Multiple Tests with Climatological Data, Journal of Climate, 17, 4343–4356, https://doi.org/10.1175/3199.1, publisher: American Meteorological Society Section: Journal of Climate, 2004.

Wade, A. R. and Parker, M. D.: Dynamics of Simulated High-Shear, Low-CAPE Supercells, Journal of the Atmospheric Sciences, 78, 1389 – 1410, https://doi.org/https://doi.org/10.1175/JAS-D-20-0117.1, place: Boston MA, USA Publisher: American Meteorological Society, 2021.

Wapler, K. and James, P.: Thunderstorm occurrence and characteristics in Central Europe under different synoptic conditions, Atmospheric Research, 158-159, 231–244, https://doi.org/10.1016/j.atmosres.2014.07.011, publisher: Elsevier B.V., 2014.

Weisman, M. L., Manning, K. W., Sobash, R. A., and Schwartz, C. S.: Simulations of Severe Convective Systems Using 1- versus 3-km Grid Spacing, Weather and Forecasting, 38, 401–423, https://doi.org/10.1175/WAF-D-22-0112.1, publisher: American Meteorological Society Section: Weather and Forecasting, 2023.

Wilhelm, L., Schwierz, C., Schröer, K., Taszarek, M., and Martius, O.: Reconstructing hail days in Switzerland with statistical models (1959–2022), Natural Hazards and Earth System Sciences, 24, 3869–3894, https://doi.org/10.5194/nhess-24-3869-2024, publisher: Copernicus GmbH, 2024.

Zeeb, A., Allen, J. T., and Van Den Broeke, M.: Understanding Left-Moving Supercells: Environmental Factors and Forecasting Challenges, under review at Weather and Forecasting, under review.

Zeeb, A. W., Ashley, W. S., Haberlie, A. M., Gensini, V. A., and Michaelis, A. C.: Supercell precipitation contribution to the United States hydroclimate, International Journal of Climatology, 44, 1489–1512, https://doi.org/10.1002/joc.8395, _eprint: https://onlinelibrary.wiley.com/doi/pdf/10.1002/joc.8395, 2024.